WARWICK
THE UNIVERSITY OF WARWICK

Manuscript version: Author's Accepted Manuscript
The version presented in WRAP is the author's accepted manuscript and may differ from the published version or Version of Record.

Persistent WRAP URL:
http://wrap.warwick.ac.uk/161014

How to cite:
Please refer to published version for the most recent bibliographic citation information. If a published version is known of, the repository item page linked to above, will contain details on accessing it.

Copyright and reuse:
The Warwick Research Archive Portal (WRAP) makes this work by researchers of the University of Warwick available open access under the following conditions.

Copyright © and all moral rights to the version of the paper presented here belong to the individual author(s) and/or other copyright owners. To the extent reasonable and practicable the material made available in WRAP has been checked for eligibility before being made available.

Copies of full items can be used for personal research or study, educational, or not-for-profit purposes without prior permission or charge. Provided that the authors, title and full bibliographic details are credited, a hyperlink and/or URL is given for the original metadata page and the content is not changed in any way.

Publisher's statement:
Please refer to the repository item page, publisher's statement section, for further information.

For more information, please contact the WRAP Team at: wrap@warwick.ac.uk.

warwick.ac.uk/lib-publications

Field-dependent band-structure measurements in two-dimensional heterostructures

Paul V Nguyen,[1] Natalie C Teutsch,[2] Nathan P Wilson,[1] Joshua Kahn,[1] Xue Xia,[2] Abigail J Graham,[2] Viktor Kandyba,[3] Alexei Barinov,[3] Xiaodong Xu,[1,4] David H Cobden,[1] Neil R Wilson[2*]*

[1]Department of Physics, University of Washington, Seattle, Washington 98195, USA

[2]Department of Physics, University of Warwick, Coventry, CV4 7AL, UK

[3]Elettra - Sincrotrone Trieste, S.C.p.A., Basovizza (TS), 34149, Italy

[4]Department of Material Science and Engineering, University of Washington, Seattle, Washington 98195, USA

Corresponding Authors

*David Cobden (cobden@uw.edu), Neil Wilson (Neil.Wilson@warwick.ac.uk)

KEYWORDS. Two-dimensional materials, two-dimensional heterostructures, two-dimensional semiconductors, angle resolved photoemission spectroscopy

ABSTRACT

In electronic and optoelectronic devices made from van der Waals heterostructures, electric fields can induce substantial band structure changes which are crucial to device operation but cannot usually be directly measured. Here, we use spatially resolved angle-resolved photoemission spectroscopy to monitor changes in band alignment of the component layers, corresponding to band structure changes of the composite heterostructure system, that are produced by electrostatic gating. Our devices comprise graphene on a monolayer semiconductor, WSe_2 or $MoSe_2$, atop a boron nitride dielectric and a graphite gate. Applying a gate voltage creates an electric field that shifts the semiconductor bands relative to those in the graphene by up to 0.2 eV. The results can be understood in simple terms by assuming that the materials do not hybridize.

Layers of van-der-Waals materials stacked in two-dimensional heterostructures (2D-HS)[1] can be used to achieve transistor operation with high on-off ratio[2,3], efficient light emission or absorption[4], and switchable phase transitions[5,6]. The electronic and opto-electronic properties of 2D-HS can be tailored by selection of the constituent layers based on their band structures and relative band alignments, as well as by control of geometry such as their relative rotation. Full working 2D electronic devices can be made by incorporating graphene or graphite as conductors, enabling application of large electric fields which modulate doping and band structure[4,7]. For electronics and optoelectronics, graphene offers distinct advantages as the metal electrodes in 2D semiconductor heterostructures; graphene is flexible, transparent, easily stacked and integrated into the heterostructure, forms interfaces to the 2D semiconductors without dangling bonds and hence enables Fermi-level depinning, and has a work-function that can be tuned by electric field[8]. As a result, the integration of graphene contacts with 2D semiconductors has shown great promise for electrical transport[9–20] and light-dependent / light-emitting 2D devices[4,21–31].

Understanding and developing such devices requires tools that probe electronic structure during device operation. For example, the band alignments at the graphene/MX_2 interface determine the the barriers to charge injection, which can change with applied electrostatic field. Although the field-dependent band structure at the graphene/MX_2 interface has been calculated by ab initio modelling[32–38], these need testing experimentally. Gate-dependent changes in optical properties are relatively straightforward to measure, but do not directly probe the electronic spectrum. Scanning tunneling spectroscopy can be combined with gating, though it reveals only momentum-integrated densities of states in the uppermost layer.[7,39,40] Efforts have been made to extract Schottky barrier heights from transport data[14,18,41,42], but these are model-dependent and indirect. On the other hand, angle-resolved photoemission spectroscopy with sub-micrometer spatial resolution (μ-ARPES) permits measurements of the full momentum-resolved electronic structure in 2D-HSs, to a depth of several layers. From this, the band alignments relative to the Fermi energy, and band offsets between layers, can be determined in mechanically exfoliated 2D heterostructures. It has recently been shown that μ-ARPES can be performed with operating gate electrodes[43–49], allowing investigation of in situ doping of the conduction band. Here we apply μ-ARPES to study electric-field induced changes in band alignments in back-gated graphene/monolayer transition metal dichalcogenide (MX_2) heterostructures.

Mechanical exfoliation and dry transfer were used to fabricate 2D-HS devices, which consist of top graphene, an MX_2 layer, a hexagonal BN dielectric (thickness D_{BN}), and a graphite back-gate electrode, as shown schematically in Figure 1a. The fabrication process was as described in earlier work,[43] using a polycarbonate film on polydimethylsiloxane stamp to pick up and align the flakes before depositing the stack on a substrate with predefined metal electrodes (Pt with Ti adhesion layer). Figure 1b is an optical microscope image of a completed device. Each device was wire-bonded in a ceramic chip carrier (8-lead side-brazed package, CSB000815 from Spectrum Semiconductor Materials Inc.) and mounted on a custom-made sample plate that allowed in-situ electrical connections at the Spectromicroscopy beamline of the ELETTRA synchrotron. Samples were annealed in ultra-high vacuum (UHV) to around 400 °C for several hours immediately prior

to transfer to the analysis chamber. Further details are given in supporting information (SI) section S1. Measurements were acquired at a sample temperature of around 100 K, with a photon energy of 27 eV. A Schwarzschild mirror was used to focus the beam down to a sub-micrometer spot and the photoemitted electrons were collected by a hemispherical analyzer mounted in the UHV chamber on a 2-axis goniometer.[50] Scanning photoemission microscopy[51] was used to find the regions of interest, where the monolayer graphene top contact overlapped both the monolayer MX_2 and the gate electrode. These areas were typically a few microns across, much bigger than the beam spot.

Angle-resolved photoemission spectra were acquired while the back-gate voltage V_G was varied *in situ* with the graphene grounded. ARPES is sensitive to the uppermost few atomic layers of the sample;[52,53] hence the spectra include photoemitted electrons from both the graphene and the underlying MX_2 layer. The hemispherical analyzer, with two-dimensional detector, was positioned to acquire spectra near the symmetry points of the Brillouin zones of the graphene and MX_2 layers, allowing analysis of the valence band dispersion in each layer. Figure 1c shows the Brillouin zones of the graphene and monolayer WSe_2, and Fig. 1d shows sketches of the bands along the three colored lines at the zone center (Γ, red), the zone corner of WSe_2 ($\mathbf{K_W}$, blue), and the zone corner of graphene ($\mathbf{K_{gr}}$, green line). The behavior of the spectra along these lines, as a function of gate voltage, is shown in the energy-momentum spectra in Figures 1e-g. As the gate voltage goes from positive to negative, the bands at each position shift up in energy. For graphene, there is a clear change from electron-doping at positive gate voltage, with the Dirac point energy below the Fermi energy, to hole doping at negative gate voltage, with the Dirac point energy above the Fermi energy. Further data are shown in SI Section S2.

At each gate voltage we determined E_Γ, the WSe_2 valence band maximum at $\mathbf{\Gamma}$, from a parabolic fit to the intense photoemission around Γ, and similarly E_K from the weaker photoemission around $\mathbf{K_W}$. The Dirac point energy, E_D, of the graphene was found from the crossing points of linear fits to each side of the conical graphene dispersion around $\mathbf{K_{gr}}$. As usual, the Fermi energy, E_F, was determined by fitting the drop in intensity across the photoemission threshold with a Fermi-Dirac distribution, and the (binding) energy is plotted relative to E_F. Further details of the data processing procedures used to extract these band edge energies are described in SI section S4. We find $E_\Gamma - E_\mathrm{K} = 0.55 \pm 0.05$ eV, and the spin splitting at $\mathbf{K_W}$ (see Fig. 1d) is $\Delta_\mathrm{SOC} = 0.48 \pm 0.03$ eV, consistent with our previous measurements[43,51] on ungated monolayer WSe_2. At $V_\mathrm{G} = 0$, the valence band edge is at $E_V = E_\mathrm{K} = -0.85 \pm 0.05$ eV, slightly below the value of -0.80 ± 0.01 eV in our previous measurements[43] where there was no top graphene.[54] Since monolayer WSe_2 on hBN has a direct gap[43] of approximately 2.1 eV, this means that the chemical potential is deep in the gap of the WSe_2. With the WSe_2 in contact with the graphene layer, and $E_V = E_\mathrm{K}$ measured relative to the Fermi level in graphene, E_K is a direct measure of the Schottky barrier height for hole injection at the graphene / WSe_2 contact. Although E_K could change depending on the density of interfacial traps and defects, more can be learnt from the dependence of E_K on V_G.

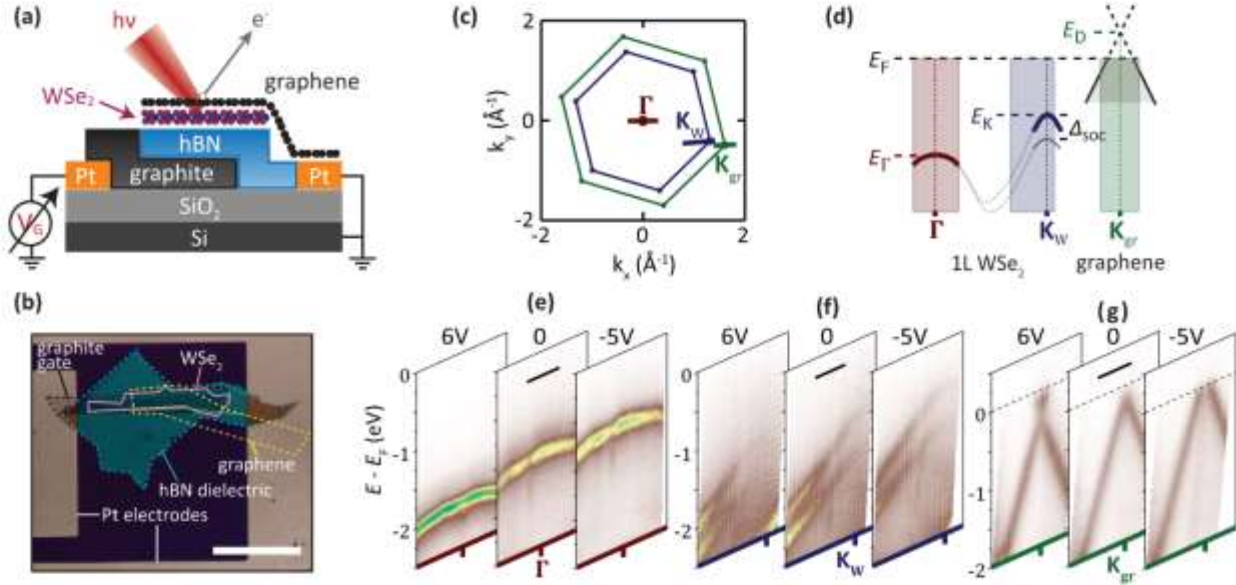

Figure 1. Gate-dependent valence band measurements in a 2D heterostructure. (a) Schematic, and (b) optical microscope image, of a 2D-HS device (graphene/WSe_2, $D_{\mathrm{BN}} = 25.5 \pm 0.2$ nm) with electrical connections made in the ARPES chamber. The scale bar is 50 µm. (c) First Brillouin zones of the monolayer WSe_2 (blue hexagon) and graphene (green hexagon), with the positions of the energy-momentum slices in the lower panels marked as solid-colored lines: red, zone center; blue, zone corner of the WSe_2; and green, zone corner of the graphene. (d) Schematic of the bands along those colored lines. Gate-dependent energy-momentum slices around $\mathbf{\Gamma}$**,** (e), $\mathbf{K_W}$, (f), and $\mathbf{K_{gr}}$, (g): gate voltages as labelled, the scale bars correspond to 0.2 Å^{-1}.

The variation of the graphene and WSe_2 band parameters with V_G is plotted in Fig. 2a. The graphene Dirac point E_D moves downwards in an S-shaped manner as V_{G} is increased, as expected due to the linearly vanishing density of states near E_{D},[8] with an overall shift of 0.6 eV. The WSe_2 valence band edges E_Γ and E_{K} also follow an S-shape, with no detectable change in $E_\Gamma - E_{\mathrm{K}}$ (nor of Δ_{SOC}); however, their overall shift is larger, at 0.8 V. It also appears that the inflection point occurs at different V_G for E_{D} and E_{K}, but this is most likely a result of spatial variations in the sample doping between the different locations where the measurements were made. Fig. 2b shows similar measurements made using a device with monolayer $MoSe_2$ instead of WSe_2. The energy-momentum slices and further device details are given in SI section S3. Spectra were only acquired from the $MoSe_2$ bands near Γ, because the photoemission intensity at the zone corner was too low. For the monolayer $MoSe_2$ device, at $V_{\mathrm{G}} = 0$, the valence band edge is at $E_{\mathrm{K}} = -1.24 \pm 0.05$ eV, lower in energy than for WSe_2. Combined with the smaller gap for $MoSe_2$ than WSe_2, this indicates slight electron-doping of the $MoSe_2$ compared to WSe_2. This could indicate a low concentration of gap states, but E_K is highly dependent on the energy of the gap states as well as their density[55], even at low densities of gap states, such that the doping level cannot be determined from E_{K} alone.

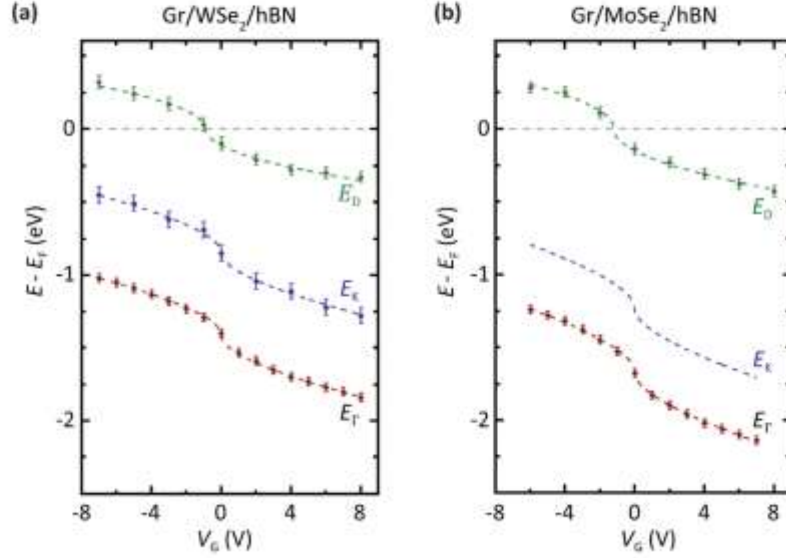

Figure 2. Gate-dependence of the band energies in graphene/MX_2 heterostructures. Values of E_{D} (green), E_{K} (blue) and E_{Γ} (maroon) extracted from the data in Figure 1, plotted as a function of V_{G}, for (a) graphene on monolayer WSe_2 ($D_{\mathrm{BN}} = 25.5 \pm 0.2$ nm) and (b) graphene on monolayer $MoSe_2$ ($D_{\mathrm{BN}} = 19.0 \pm 0.5$ nm). The dashed lines are fits to the data as described in the text. In (b), E_{K} is calculated from the fit to E_{Γ} assuming a constant energy difference of $E_{\Gamma} - E_{\mathrm{K}}$= 0.44 eV. The data processing procedures used to extract these band edge energies are described in SI section S4.

We can interpret these band shifts using the schematic band diagrams shown in Fig. 3. No signs of hybridization are evident, so we treat the bands in the WSe_2 and graphene as separate. At $V_{\mathrm{G}} = 0$ (Fig. 3a), for both WSe_2 and $MoSe_2$, the graphene Dirac point E_{D} is very close to the Fermi level (zero), implying that the graphene is undoped and the electric field in the hBN is small. The position of the valence band edge E_{K} in the monolayer MX_2 at that condition is defined to be E_{K0}.

Under a positive gate voltage V_{G} applied to the graphite (Fig. 3b) there is an electric field in the hBN and the graphene is doped with electrons such that $E_{\mathrm{D}} = -\mu$, where μ is the chemical potential in the graphene. The total areal charge density in the graphene plus MX_2 is to a good approximation CV_{G}, where $C = \epsilon_{\mathrm{BN}}/D$ is the geometric capacitance of the hBN with thickness D_{BN} and dielectric constant[43] ϵ_{BN}. Thus $e\int_0^{\mu} n(E)dE \approx CV_{\mathrm{G}}$, where e is the magnitude of the electron charge and $n(E) = n_{gr} + n_{gap}$ is the sum of the density of states of the graphene, $n_{gr} = \frac{2}{\pi(\hbar v_F)^2}E$, and of in-gap states in the MX_2, n_{gap}. For the WSe_2 device ($D_{\mathrm{BN}} = 25.5 \pm 0.2$ nm) we obtain a good fit to the measurements of E_D vs V_G by taking $n_{gap} = 0$ (green dashed line in Fig. 2a), and we can infer that n_{gap} in the monolayer WSe_2 is less than 10^{11} cm^{-2} consistent with previous reports that have also found a low density of traps and gap states at the MX_2/BN interface[55,56].

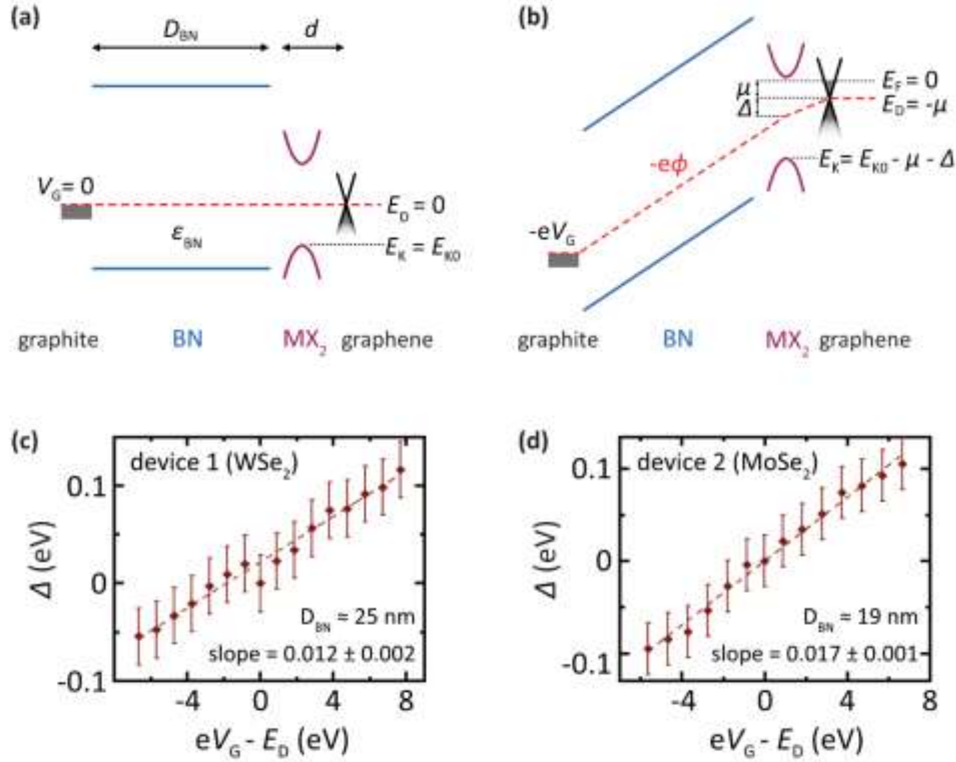

Figure 3. Inferring the gate-dependent electrostatic potential drop, Δ, between the MX_2 and the graphene. (a) and (b), Schematic band diagrams across the heterostructure at zero and positive gate voltage V_G, respectively. (c) and (d), The electrostatic potential difference between states in the MX_2 and the top graphene layer, determined from the band alignment data in Figure 2, plotted as a function of the electrostatic potential drop across the hBN for WSe_2 and $MoSe_2$ heterostructures, respectively. The dashed lines are linear fits to the data. Further details on determining Δ are described in SI section S4.

To understand the band shifts in the MX_2 layer, both the change in chemical potential in the graphene, and hence its change in work-function,[8] and the electric field across the heterostructure must be considered. With the MX_2 layer in contact with the graphene, the MX_2 valence band edges shift with E_D and hence also follow an apparent S-shape. But their overall shift is larger than the shift in E_D: the shift of the MX_2 bands relative to the graphene Dirac point observed in Figs. 1 and 2 is a natural consequence of the gate electric field. Some of the electric flux passes through the MX_2 and terminates on the graphene, creating an electrostatic potential energy difference Δ between the electron states in the MX_2 and those in the graphene. In Fig. 3b we use a red dashed line to indicate the corresponding variation of the electrostatic potential ϕ across the stack. (The change in slope at the MX_2 layer corresponds to polarization charge in the dielectrics plus the charge in in-gap states). The total potential drop across the heterostructure is equal to the electrostatic potential drop plus the change in chemical potential in the graphene layer, sometimes

described as adding the geometric capacitance in series with the quantum capacitance of the graphene layer[8]. Assuming the polarization of the insulators is in linear response, Δ will be proportional to the total potential drop $(V_G - \mu/e)$ between the gate and the graphene, that is, $\Delta = \alpha(eV_G - \mu)$, where α is a numerical constant. From Fig. 3b one can see that $E_K = E_{K0} - \mu - \Delta$ and so, using $\mu = -E_D$,

$$\Delta = E_{K0} - E_K + E_D = \alpha(eV_G - E_D)\,.$$

Therefore, a plot of $\Delta = E_{K0} - E_K + E_D$ versus $eV_G - E_D$ should yield a straight line of slope α. Such plots for both WSe_2 (Fig. 3c) and $MoSe_2$ (Fig. 3d) devices do indeed yield straight lines whose best fit slopes are $\alpha = 0.012 \pm 0.002$ and 0.017 ± 0.001 respectively. (In making these plots we compensated for the doping inhomogeneity; see SI section S4).

To see that these measured values of α are reasonable, let us consider a layered capacitor containing a hBN slab of thickness D_{BN} and an MX_2 slab of thickness $d \ll D_{BN}$. The fraction of the potential applied to the capacitor that drops across the MX_2 slab is $\alpha' \approx \frac{d}{D_{BN}}\frac{\epsilon_{BN}}{\epsilon_M}$, where ϵ_M is the dielectric constant of the MX_2. Taking d as the monolayer spacing which is 0.65 nm[57–60], $\epsilon_M \approx 10$, $\epsilon_{BN} \approx 4$, and $D_{BN} \approx 25$ nm (as in the WSe_2 device) gives $\alpha' \approx 0.014$. Using $D_{BN} \approx 19$ nm (as in the $MoSe_2$ device) gives $\alpha' \approx 0.018$. Although this is only a very rough model of our structure, these estimates of α' are consistent with the measured values of α, implying that the dielectric-slab approach gives a practical way to estimate electric-field induced band shifts in heterostructures.

With the validation given by the results presented here, we expect this dielectric-slab approach to be generically applicable for estimating band shifts in other 2D heterostructures as long as interactions between the layers are weak. The quantitative predictions of this model will enable device design to optimize changes in Schottky barrier height and hence increase the ON/OFF ratio in graphene-contacted MX_2 field effect transistors[33], for example. The model does not consider interactions between layers such that, for example, it does not depend on the twist-angle between the graphene and MX_2 layers. With the significant difference in lattice parameter between graphene (0.25 nm) and monolayer MX_2 (0.33 nm), a moiré superlattice potential is not expected. In systems where moiré effects change the density of states near the Fermi energy, these would need to be considered and could be probed by field-dependent band structure measurements using μ-ARPES.

In conclusion, we have demonstrated that μ-ARPES can be used to observe and quantify changes induced by an applied electric field in the band structure of 2D heterostructures. The changes we observed correspond to simple shifts of the bands associated with component monolayers which do not significantly hybridize (graphene/MX_2), and illustrate the significance of the sequence of the layers[32] as well as their individual properties. This being established, the technique can in the future be applied to gain insights into other heterostructures that host hybridized bands and moiré superlattices, such as the flat bands associated with diverse correlated and topological states in multilayer graphene and MX_2/$M'X'_2$ with appropriate twist angles.

ASSOCIATED CONTENT

Supporting Information. Sample fabrication and preparation; gate dependent spectra from graphene on monolayer WSe_2 heterostructure; sample details and gate-dependent spectra from graphene on monolayer $MoSe_2$ heterostructure; further details on determining the electrostatic potential drop across the MX_2 layer.

AUTHOR INFORMATION

Corresponding Author

David Cobden (cobden@uw.edu), Neil Wilson (Neil.Wilson@warwick.ac.uk)

Author Contributions

The manuscript was written with contributions from all authors.

ACKNOWLEDGMENT

Research on monitoring gated electronic structure changes is supported as part of Programmable Quantum Materials, an Energy Frontier Research Center funded by the U.S. Department of Energy (DOE), Office of Science, Basic Energy Sciences (BES), under award DE-SC0019443. N.R.W. and N.D.M.H. were supported through U.K. Engineering and Physical Sciences Research Council (EPSRC) award EP/P01139X/1. N.C.T., N.Y. and A.J.G. were supported through EPSRC studentships (EP/M508184/1 and EP/R513374/1). X.Xia was supported by a University of Warwick studentship. We thank Gabriel Constantinescu and Nicholas Hine for helpful discussions.

References

(1) Novoselov, K. S.; Mishchenko, A.; Carvalho, A.; Castro Neto, A. H. 2D Materials and van Der Waals Heterostructures. *Science (80-.).* **2016**, *353* (6298), aac9439. https://doi.org/10.1126/science.aac9439.

(2) Britnell, L.; Gorbachev, R. V.; Jalil, R.; Belle, B. D.; Schedin, F.; Mishchenko, A.; Georgiou, T.; Katsnelson, M. I.; Eaves, L.; Morozov, S. V.; Peres, N. M. R.; Leist, J.; Geim, A. K.; Novoselov, K. S.; Ponomarenko, L. a. Field-Effect Tunneling Transistor Based on Vertical Graphene Heterostructures. *Science (80-.).* **2012**, *335* (6071), 947–950. https://doi.org/10.1126/science.1218461.

(3) Liu, Y.; Duan, X.; Shin, H. J.; Park, S.; Huang, Y.; Duan, X. Promises and Prospects of Two-Dimensional Transistors. *Nature* **2021**, *591* (7848), 43–53. https://doi.org/10.1038/s41586-021-

03339-z.

(4) Withers, F.; Del Pozo-Zamudio, O.; Mishchenko, A.; Rooney, a. P.; Gholinia, A.; Watanabe, K.; Taniguchi, T.; Haigh, S. J.; Geim, a. K.; Tartakovskii, a. I.; Novoselov, K. S. Light-Emitting Diodes by Band-Structure Engineering in van Der Waals Heterostructures. *Nat. Mater.* **2015**, *14* (3), 301–306. https://doi.org/10.1038/nmat4205.

(5) Cao, Y.; Fatemi, V.; Fang, S.; Watanabe, K.; Taniguchi, T.; Kaxiras, E.; Jarillo-Herrero, P. Unconventional Superconductivity in Magic-Angle Graphene Superlattices. *Nature* **2018**, *556* (7699), 43–50. https://doi.org/10.1038/nature26160.

(6) Cao, Y.; Fatemi, V.; Demir, A.; Fang, S.; Tomarken, S. L.; Luo, J. Y.; Sanchez-Yamagishi, J. D.; Watanabe, K.; Taniguchi, T.; Kaxiras, E.; Ashoori, R. C.; Jarillo-Herrero, P. Correlated Insulator Behaviour at Half-Filling in Magic-Angle Graphene Superlattices. *Nature* **2018**, *556* (7699), 80–84. https://doi.org/10.1038/nature26154.

(7) Liu, Y.; Qiu, Z.; Carvalho, A.; Bao, Y.; Xu, H.; Tan, S. J. R.; Liu, W.; Castro Neto, A. H.; Loh, K. P.; Lu, J. Gate-Tunable Giant Stark Effect in Few-Layer Black Phosphorus. *Nano Lett.* **2017**, *17* (3), 1970–1977. https://doi.org/10.1021/acs.nanolett.6b05381.

(8) Yu, Y.-J.; Zhao, Y.; Ryu, S.; Brus, L. E.; Kim, K. S.; Kim, P. Tuning the Graphene Work Function by Electric Field Effect. *Nano Lett.* **2009**, *9* (10), 3430–3434. https://doi.org/10.1021/nl901572a.

(9) Liu, Y.; Wu, H.; Cheng, H.-C.; Yang, S.; Zhu, E.; He, Q.; Ding, M.; Li, D.; Guo, J.; Weiss, N. O.; Huang, Y.; Duan, X. Toward Barrier Free Contact to Molybdenum Disulfide Using Graphene Electrodes. *Nano Lett.* **2015**, *15* (5), 3030–3034. https://doi.org/10.1021/nl504957p.

(10) Cui, X.; Lee, G.-H.; Kim, Y. D.; Arefe, G.; Huang, P. Y.; Lee, C.-H.; Chenet, D. A.; Zhang, X.; Wang, L.; Ye, F.; Pizzocchero, F.; Jessen, B. S.; Watanabe, K.; Taniguchi, T.; Muller, D. A.; Low, T.; Kim, P.; Hone, J. Multi-Terminal Transport Measurements of MoS2 Using a van Der Waals Heterostructure Device Platform. *Nat. Nanotechnol.* **2015**, *10* (6), 534–540. https://doi.org/10.1038/nnano.2015.70.

(11) Shih, C.-J.; Wang, Q. H.; Son, Y.; Jin, Z.; Blankschtein, D.; Strano, M. S. Tuning On–Off Current Ratio and Field-Effect Mobility in a MoS 2 –Graphene Heterostructure via Schottky Barrier Modulation. *ACS Nano* **2014**, *8* (6), 5790–5798. https://doi.org/10.1021/nn500676t.

(12) Georgiou, T.; Jalil, R.; Belle, B. D.; Britnell, L.; Gorbachev, R. V.; Morozov, S. V.; Kim, Y.-J.; Gholinia, A.; Haigh, S. J.; Makarovsky, O.; Eaves, L.; Ponomarenko, L. A.; Geim, A. K.; Novoselov, K. S.; Mishchenko, A. Vertical Field-Effect Transistor Based on Graphene–WS2 Heterostructures for Flexible and Transparent Electronics. *Nat. Nanotechnol.* **2013**, *8* (2), 100–103. https://doi.org/10.1038/nnano.2012.224.

(13) Seo, D.; Lee, D. Y.; Kwon, J.; Lee, J. J.; Taniguchi, T.; Watanabe, K.; Lee, G.-H.; Kim, K. S.; Hone, J.; Kim, Y. D.; Choi, H.-J. High-Performance Monolayer MoS 2 Field-Effect Transistor with Large-Scale Nitrogen-Doped Graphene Electrodes for Ohmic Contact. *Appl. Phys. Lett.* **2019**, *115* (1), 012104. https://doi.org/10.1063/1.5094682.

(14) Larentis, S.; Tolsma, J. R.; Fallahazad, B.; Dillen, D. C.; Kim, K.; Macdonald, A. H.; Tutuc, E. Band Offset and Negative Compressibility in Graphene-MoS2 Heterostructures. *Nano Lett.* **2014**, *14* (4), 2039–2045. https://doi.org/10.1021/nl500212s.

(15) Tian, H.; Tan, Z.; Wu, C.; Wang, X.; Mohammad, M. A.; Xie, D.; Yang, Y.; Wang, J.; Li, L.-J.; Xu, J.; Ren, T.-L. Novel Field-Effect Schottky Barrier Transistors Based on Graphene-MoS2 Heterojunctions. *Sci. Rep.* **2015**, *4* (1), 5951. https://doi.org/10.1038/srep05951.

(16) Allain, A.; Kang, J.; Banerjee, K.; Kis, A. Electrical Contacts to Two-Dimensional Semiconductors. *Nat. Mater.* **2015**, *14* (12), 1195–1205. https://doi.org/10.1038/nmat4452.

(17) Xie, L.; Liao, M.; Wang, S.; Yu, H.; Du, L.; Tang, J.; Zhao, J.; Zhang, J.; Chen, P.; Lu, X.; Wang, G.; Xie, G.; Yang, R.; Shi, D.; Zhang, G. Graphene-Contacted Ultrashort Channel Monolayer MoS 2 Transistors. *Adv. Mater.* **2017**, *29* (37), 1702522. https://doi.org/10.1002/adma.201702522.

(18) LaGasse, S. W.; Dhakras, P.; Watanabe, K.; Taniguchi, T.; Lee, J. U. Gate-Tunable Graphene–WSe 2 Heterojunctions at the Schottky–Mott Limit. *Adv. Mater.* **2019**, *31* (24), 1901392. https://doi.org/10.1002/adma.201901392.

(19) Jin, Y.; Joo, M.-K.; Moon, B. H.; Kim, H.; Lee, S.; Jeong, H. Y.; Lee, Y. H. Coulomb Drag Transistor Using a Graphene and MoS2 Heterostructure. *Commun. Phys.* **2020**, *3* (1), 189. https://doi.org/10.1038/s42005-020-00461-8.

(20) Roy, T.; Tosun, M.; Kang, J. S.; Sachid, A. B.; Desai, S. B.; Hettick, M.; Hu, C. C.; Javey, A. Field-Effect Transistors Built from All Two-Dimensional Material Components. *ACS Nano* **2014**, *8* (6), 6259–6264. https://doi.org/10.1021/nn501723y.

(21) Britnell, L.; Ribeiro, R. M.; Eckmann, A.; Jalil, R.; Belle, B. D.; Mishchenko, A.; Kim, Y.-J.; Gorbachev, R. V; Georgiou, T.; Morozov, S. V; Grigorenko, A. N.; Geim, A. K.; Casiraghi, C.; Neto, A. H. C.; Novoselov, K. S. Strong Light-Matter Interactions in Heterostructures of Atomically Thin Films. *Science (80-.).* **2013**, *340* (6138), 1311–1314. https://doi.org/10.1126/science.1235547.

(22) Song, T.; Fei, Z.; Yankowitz, M.; Lin, Z.; Jiang, Q.; Hwangbo, K.; Zhang, Q.; Sun, B.; Taniguchi, T.; Watanabe, K.; McGuire, M. A.; Graf, D.; Cao, T.; Chu, J. H.; Cobden, D. H.; Dean, C. R.; Xiao, D.; Xu, X. Switching 2D Magnetic States via Pressure Tuning of Layer Stacking. *Nat. Mater.* **2019**, *18* (12), 1298–1302. https://doi.org/10.1038/s41563-019-0505-2.

(23) Zhou, X.; Hu, X.; Yu, J.; Liu, S.; Shu, Z.; Zhang, Q.; Li, H.; Ma, Y.; Xu, H.; Zhai, T. 2D Layered Material-Based van Der Waals Heterostructures for Optoelectronics. *Adv. Funct. Mater.* **2018**, *28* (14), 1706587. https://doi.org/10.1002/adfm.201706587.

(24) Yu, W. J.; Liu, Y.; Zhou, H.; Yin, A.; Li, Z.; Huang, Y.; Duan, X. Highly Efficient Gate-Tunable Photocurrent Generation in Vertical Heterostructures of Layered Materials. *Nat. Nanotechnol.* **2013**, *8* (12), 952–958. https://doi.org/10.1038/nnano.2013.219.

(25) Xu, H.; Wu, J.; Feng, Q.; Mao, N.; Wang, C.; Zhang, J. High Responsivity and Gate Tunable Graphene-MoS 2 Hybrid Phototransistor. *Small* **2014**, *10* (11), 2300–2306. https://doi.org/10.1002/smll.201303670.

(26) Yu, W. J.; Vu, Q. A.; Oh, H.; Nam, H. G.; Zhou, H.; Cha, S.; Kim, J.-Y.; Carvalho, A.; Jeong, M.; Choi, H.; Castro Neto, A. H.; Lee, Y. H.; Duan, X. Unusually Efficient Photocurrent Extraction in Monolayer van Der Waals Heterostructure by Tunnelling through Discretized Barriers. *Nat. Commun.* **2016**, *7* (1), 13278. https://doi.org/10.1038/ncomms13278.

(27) Massicotte, M.; Schmidt, P.; Vialla, F.; Schädler, K. G.; Reserbat-Plantey, A.; Watanabe, K.;

Taniguchi, T.; Tielrooij, K. J.; Koppens, F. H. L. Picosecond Photoresponse in van Der Waals Heterostructures. *Nat. Nanotechnol.* **2016**, *11* (1), 42–46. https://doi.org/10.1038/nnano.2015.227.

(28) Liu, C.-H.; Clark, G.; Fryett, T.; Wu, S.; Zheng, J.; Hatami, F.; Xu, X.; Majumdar, A. Nanocavity Integrated van Der Waals Heterostructure Light-Emitting Tunneling Diode. *Nano Lett.* **2017**, *17* (1), 200–205. https://doi.org/10.1021/acs.nanolett.6b03801.

(29) Del Pozo-Zamudio, O.; Genco, A.; Schwarz, S.; Withers, F.; Walker, P. M.; Godde, T.; Schofield, R. C.; Rooney, A. P.; Prestat, E.; Watanabe, K.; Taniguchi, T.; Clark, C.; Haigh, S. J.; Krizhanovskii, D. N.; Novoselov, K. S.; Tartakovskii, A. I. Electrically Pumped WSe 2 -Based Light-Emitting van Der Waals Heterostructures Embedded in Monolithic Dielectric Microcavities. *2D Mater.* **2020**, *7* (3), 031006. https://doi.org/10.1088/2053-1583/ab8542.

(30) Roy, K.; Padmanabhan, M.; Goswami, S.; Sai, T. P.; Kaushal, S.; Ghosh, A. Optically Active Heterostructures of Graphene and Ultrathin MoS2. *Solid State Commun.* **2013**, *175–176*, 35–42. https://doi.org/10.1016/j.ssc.2013.09.021.

(31) Luo, D.; Tang, J.; Shen, X.; Ji, F.; Yang, J.; Weathersby, S.; Kozina, M. E.; Chen, Z.; Xiao, J.; Ye, Y.; Cao, T.; Zhang, G.; Wang, X.; Lindenberg, A. M. Twist-Angle-Dependent Ultrafast Charge Transfer in MoS 2 -Graphene van Der Waals Heterostructures. *Nano Lett.* **2021**, *21* (19), 8051–8057. https://doi.org/10.1021/acs.nanolett.1c02356.

(32) Stradi, D.; Papior, N. R.; Hansen, O.; Brandbyge, M. Field Effect in Graphene-Based van Der Waals Heterostructures: Stacking Sequence Matters. *Nano Lett.* **2017**, *17* (4), 2660–2666. https://doi.org/10.1021/acs.nanolett.7b00473.

(33) Baik, S. S.; Im, S.; Choi, H. J. Work Function Tuning in Two-Dimensional MoS2 Field-Effect-Transistors with Graphene and Titanium Source-Drain Contacts. *Sci. Rep.* **2017**, *7* (1), 45546. https://doi.org/10.1038/srep45546.

(34) Zhang, R.; Hao, G.; Ye, X.; Gao, S.; Li, H. Tunable Electronic Properties and Schottky Barrier in a Graphene/WSe 2 Heterostructure under out-of-Plane Strain and an Electric Field. *Phys. Chem. Chem. Phys.* **2020**, *22* (41), 23699–23706. https://doi.org/10.1039/D0CP04160B.

(35) Zheng, J.; Li, E.; Ma, D.; Cui, Z.; Peng, T.; Wang, X. Effect on Schottky Barrier of Graphene/WS 2 Heterostructure With Vertical Electric Field and Biaxial Strain. *Phys. status solidi* **2019**, *256* (10), 1900161. https://doi.org/10.1002/pssb.201900161.

(36) Zhang, W.; Hao, G.; Zhang, R.; Xu, J.; Ye, X.; Li, H. Effects of Vertical Strain and Electrical Field on Electronic Properties and Schottky Contact of Graphene/MoSe2 Heterojunction. *J. Phys. Chem. Solids* **2021**, *157* (February), 110189. https://doi.org/10.1016/j.jpcs.2021.110189.

(37) Pham, K. D.; Hieu, N. N.; Phuc, H. V.; Hoi, B. D.; Ilysov, V. V.; Amin, B.; Nguyen, C. V. First Principles Study of the Electronic Properties and Schottky Barrier in Vertically Stacked Graphene on the Janus MoSeS under Electric Field. *Comput. Mater. Sci.* **2018**, *153* (May), 438–444. https://doi.org/10.1016/j.commatsci.2018.07.017.

(38) Nguyen, C. V. Tuning the Electronic Properties and Schottky Barrier Height of the Vertical Graphene/MoS 2 Heterostructure by an Electric Gating. *Superlattices Microstruct.* **2018**, *116*, 79–87. https://doi.org/10.1016/j.spmi.2018.02.012.

(39) Lu, C.-P.; Li, G.; Mao, J.; Wang, L.-M.; Andrei, E. Y. Bandgap, Mid-Gap States, and Gating Effects in MoS2. *Nano Lett.* **2014**, *14* (8), 4628–4633. https://doi.org/10.1021/nl501659n.

(40) Zhang, Y.; Brar, V. W.; Wang, F.; Girit, C.; Yayon, Y.; Panlasigui, M.; Zettl, A.; Crommie, M. F. Giant Phonon-Induced Conductance in Scanning Tunnelling Spectroscopy of Gate-Tunable Graphene. *Nat. Phys.* **2008**, *4* (8), 627–630. https://doi.org/10.1038/nphys1022.

(41) Murali, K.; Dandu, M.; Watanabe, K.; Taniguchi, T.; Majumdar, K. Accurate Extraction of Schottky Barrier Height and Universality of Fermi Level De-Pinning of van Der Waals Contacts. *Adv. Funct. Mater.* **2021**, *31* (18), 2010513. https://doi.org/10.1002/adfm.202010513.

(42) Van Nguyen, K.; Lin, S.-Y.; Chang, Y.-C. Transfer Current in P-Type Graphene/MoS2 Heterostructures. *Phys. E Low-dimensional Syst. Nanostructures* **2021**, *125* (July 2020), 114383. https://doi.org/10.1016/j.physe.2020.114383.

(43) Nguyen, P. V.; Teutsch, N. C.; Wilson, N. R. N. P. N. R.; Kahn, J.; Xia, X.; Graham, A. J.; Kandyba, V.; Giampietri, A.; Barinov, A.; Constantinescu, G. C.; Yeung, N.; Hine, N. D. M.; Xu, X.; Cobden, D. H.; Wilson, N. R. N. P. N. R. Visualizing Electrostatic Gating Effects in Two-Dimensional Heterostructures. *Nature* **2019**, *572* (7768), 220–223. https://doi.org/10.1038/s41586-019-1402-1.

(44) Joucken, F.; Avila, J.; Ge, Z.; Quezada-Lopez, E. A.; Yi, H.; Le Goff, R.; Baudin, E.; Davenport, J. L.; Watanabe, K.; Taniguchi, T.; Asensio, M. C.; Velasco, J. Visualizing the Effect of an Electrostatic Gate with Angle-Resolved Photoemission Spectroscopy. *Nano Lett.* **2019**, *19* (4), 2682–2687. https://doi.org/10.1021/acs.nanolett.9b00649.

(45) Hofmann, P. Accessing the Spectral Function of in Operando Devices by Angle-Resolved Photoemission Spectroscopy. *AVS Quantum Sci.* **2021**, *3* (2), 021101. https://doi.org/10.1116/5.0038637.

(46) Majchrzak, P.; Muzzio, R.; Jones, A. J. H.; Curcio, D.; Volckaert, K.; Biswas, D.; Gobbo, J.; Singh, S.; Robinson, J. T.; Watanabe, K.; Taniguchi, T.; Kim, T. K.; Cacho, C.; Miwa, J. A.; Hofmann, P.; Katoch, J.; Ulstrup, S. In Operando Angle-Resolved Photoemission Spectroscopy with Nanoscale Spatial Resolution: Spatial Mapping of the Electronic Structure of Twisted Bilayer Graphene. *Small Sci.* **2021**, *1* (6), 2000075. https://doi.org/10.1002/smsc.202000075.

(47) Jones, A. J. H.; Muzzio, R.; Majchrzak, P.; Pakdel, S.; Curcio, D.; Volckaert, K.; Biswas, D.; Gobbo, J.; Singh, S.; Robinson, J. T.; Watanabe, K.; Taniguchi, T.; Kim, T. K.; Cacho, C.; Lanata, N.; Miwa, J. A.; Hofmann, P.; Katoch, J.; Ulstrup, S. Observation of Electrically Tunable van Hove Singularities in Twisted Bilayer Graphene from NanoARPES. *Adv. Mater.* **2020**, *32* (31), 1–7. https://doi.org/10.1002/adma.202001656.

(48) Curcio, D.; Jones, A. J. H.; Muzzio, R.; Volckaert, K.; Biswas, D.; Sanders, C. E.; Dudin, P.; Cacho, C.; Singh, S.; Watanabe, K.; Taniguchi, T.; Miwa, J. A.; Katoch, J.; Ulstrup, S.; Hofmann, P. Accessing the Spectral Function in a Current-Carrying Device. *Phys. Rev. Lett.* **2020**, *125* (23), 1–9. https://doi.org/10.1103/PhysRevLett.125.236403.

(49) Muzzio, R.; Jones, A. J. H.; Curcio, D.; Biswas, D.; Miwa, J. A.; Hofmann, P.; Watanabe, K.; Taniguchi, T.; Singh, S.; Jozwiak, C.; Rotenberg, E.; Bostwick, A.; Koch, R. J.; Ulstrup, S.; Katoch, J. Momentum-Resolved View of Highly Tunable Many-Body Effects in a Graphene/HBN Field-Effect

Device. *Phys. Rev. B* **2020**, *101* (20), 201409. https://doi.org/10.1103/PhysRevB.101.201409.

(50) Dudin, P.; Lacovig, P.; Fava, C.; Nicolini, E.; Bianco, A.; Cautero, G.; Barinov, A. Angle-Resolved Photoemission Spectroscopy and Imaging with a Submicrometre Probe at the SPECTROMICROSCOPY-3.2L Beamline of Elettra. *J. Synchrotron Radiat.* **2010**, *17* (4), 445–450. https://doi.org/10.1107/S0909049510013993.

(51) Wilson, N. R.; Nguyen, P. V.; Seyler, K.; Rivera, P.; Marsden, A. J.; Laker, Z. P. L.; Constantinescu, G. C.; Kandyba, V.; Barinov, A.; Hine, N. D. M.; Xu, X.; Cobden, D. H. Determination of Band Offsets, Hybridization, and Exciton Binding in 2D Semiconductor Heterostructures. *Sci. Adv.* **2017**, *3* (2), e1601832. https://doi.org/10.1126/sciadv.1601832.

(52) Seah, M. P.; Dench, W. A. Quantitative Electron Spectroscopy of Surfaces: A Standard Data Base for Electron Inelastic Mean Free Paths in Solids. *Surf. Interface Anal.* **1979**, *1* (1), 2–11. https://doi.org/10.1002/sia.740010103.

(53) Damascelli, A. Probing the Electronic Structure of Complex Systems by ARPES. *Phys. Scr.* **2004**, *T109*, 61. https://doi.org/10.1238/Physica.Topical.109a00061.

(54) Raja, A.; Chaves, A.; Yu, J.; Arefe, G.; Hill, H. M.; Rigosi, A. F.; Berkelbach, T. C.; Nagler, P.; Schüller, C.; Korn, T.; Nuckolls, C.; Hone, J.; Brus, L. E.; Heinz, T. F.; Reichman, D. R.; Chernikov, A. Coulomb Engineering of the Bandgap and Excitons in Two-Dimensional Materials. *Nat. Commun.* **2017**, *8* (May), 15251. https://doi.org/10.1038/ncomms15251.

(55) Ali, F.; Ahmed, F.; Taqi, M.; Mitta, S. B.; Ngo, T. D.; Eom, D. J.; Watanabe, K.; Taniguchi, T.; Kim, H.; Hwang, E.; Yoo, W. J. Traps at the HBN/WSe2 Interface and Their Impact on Polarity Transition in WSe2. *2D Mater.* **2021**, *8* (3). https://doi.org/10.1088/2053-1583/abf98d.

(56) Vu, Q. A.; Fan, S.; Lee, S. H.; Joo, M.-K.; Yu, W. J.; Lee, Y. H. Near-Zero Hysteresis and near-Ideal Subthreshold Swing in h-BN Encapsulated Single-Layer MoS 2 Field-Effect Transistors. *2D Mater.* **2018**, *5* (3), 031001. https://doi.org/10.1088/2053-1583/aab672.

(57) Fang, H.; Chuang, S.; Chang, T. C.; Takei, K.; Takahashi, T.; Javey, A. High-Performance Single Layered WSe 2 p-FETs with Chemically Doped Contacts. *Nano Lett.* **2012**, *12* (7), 3788–3792. https://doi.org/10.1021/nl301702r.

(58) Huang, J.-K.; Pu, J.; Hsu, C.-L.; Chiu, M.-H.; Juang, Z.-Y.; Chang, Y.-H.; Chang, W.-H.; Iwasa, Y.; Takenobu, T.; Li, L.-J. Large-Area Synthesis of Highly Crystalline WSe 2 Monolayers and Device Applications. *ACS Nano* **2014**, *8* (1), 923–930. https://doi.org/10.1021/nn405719x.

(59) Li, Y.; Chernikov, A.; Zhang, X.; Rigosi, A.; Hill, H. M.; van der Zande, A. M.; Chenet, D. A.; Shih, E.-M.; Hone, J.; Heinz, T. F. Measurement of the Optical Dielectric Function of Monolayer Transition-Metal Dichalcogenides: MoS 2 , Mo S e 2 , WS 2 , and WS e 2. *Phys. Rev. B* **2014**, *90* (20), 205422. https://doi.org/10.1103/PhysRevB.90.205422.

(60) Kim, K.; Larentis, S.; Fallahazad, B.; Lee, K.; Xue, J.; Dillen, D. C.; Corbet, C. M.; Tutuc, E. Band Alignment in WSe_2–Graphene Heterostructures. *ACS Nano* **2015**, *9* (4), 4527–4532. https://doi.org/10.1021/acsnano.5b01114.

Table of Contents Graphic, for Table of Contents Only